Programming Hierarchical Self-Assembly of Patchy Particles into Colloidal Crystals via Colloidal Molecules

Morphew, Daniel; Shaw, James; Avins, Christopher; Chakrabarti, Dwaipayan

DOI:
10.1021/acsnano.7b07633

Document Version
Publisher's PDF, also known as Version of record

Citation for published version (Harvard):
Morphew, D, Shaw, J, Avins, C & Chakrabarti, D 2018, 'Programming Hierarchical Self-Assembly of Patchy Particles into Colloidal Crystals *via* Colloidal Molecules', *ACS Nano*, vol. 12, no. 3, pp. 2355-2364. https://doi.org/10.1021/acsnano.7b07633

ACS NANO

Cite This: ACS Nano 2018, 12, 2355−2364

www.acsnano.org

ARTICLE

Programming Hierarchical Self-Assembly of Patchy Particles into Colloidal Crystals *via* Colloidal Molecules

Daniel Morphew, James Shaw, Christopher Avins, and Dwaipayan Chakrabarti*

School of Chemistry, University of Birmingham, Edgbaston, Birmingham B15 2TT, U.K.

Supporting Information

ABSTRACT: **Colloidal self-assembly is a promising bottom-up route to a wide variety of three-dimensional structures, from clusters to crystals. Programming hierarchical self-assembly of colloidal building blocks, which can give rise to structures ordered at multiple levels to rival biological complexity, poses a multiscale design problem. Here we explore a generic design principle that exploits a hierarchy of interaction strengths and employ this design principle in computer simulations to demonstrate the hierarchical self-assembly of triblock patchy colloidal particles into two distinct colloidal crystals. We obtain cubic diamond and body-centered cubic crystals *via* distinct clusters of uniform size and shape, namely, tetrahedra and octahedra, respectively. Such a conceptual design framework has the potential to reliably encode hierarchical self-assembly of colloidal particles into a high level of sophistication. Moreover, the design framework underpins a bottom-up route to cubic diamond colloidal crystals, which have remained elusive despite being much sought after for their attractive photonic applications.**

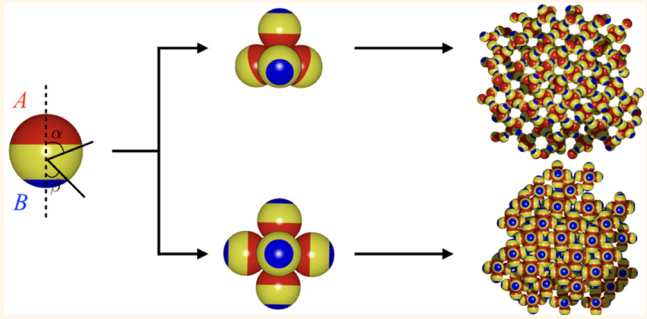

KEYWORDS: *colloidal self-assembly, hierarchical self-assembly, patchy particles, colloidal molecules, colloidal crystals, cubic diamond lattice*

The scope for tuning the interactions between colloidal particles offers enormous opportunity to program their self-assembly.[1−3] In particular, hierarchical self-assembly of colloidal particles, which is currently at an early stage of exploration,[4−10] offers a bottom-up route to an increased level of structural complexity. However, programming hierarchical self-assembly faces a major challenge in bridging hierarchies of multiple length- and time-scales associated with structure and dynamics, respectively, along the self-assembly pathways.[11] While hierarchical self-assembly of colloidal particles *via* small colloidal clusters mimicking the symmetry of molecular structures, *i.e.*, the so-called "colloidal molecules",[11−14] could be a plausible route to structural hierarchy, hierarchical schemes for programmed colloidal self-assembly have been elusive.[4,5] Another major challenge that such a route faces is to assemble the colloidal molecules in a self-limiting way for them to serve as uniform secondary building blocks for the next level of assembly.[15,16]

A recent study examined the kinetic accessibility of a series of hollow spherical structures with a two-level structural hierarchy self-assembled from charge-stabilized colloidal magnetic particles.[17] The study reports that for a staged assembly pathway, the structure, which derives the strongest energetic stability from the first stage of assembly and the weakest from the second stage, is most kinetically accessible. In this context, we explored a route that exploits a hierarchy of interaction strengths to encode structural hierarchy.[16,18] In the present study, we realized a hierarchy of interaction strengths with triblock patchy colloidal particles. Our designer patchy particles are spherical in shape, having two distinct attractive patches, A and B, at the poles across a charged band in the middle. Such triblock spherical particles were recently synthesized at the micrometer scale and shown to undergo staged assembly triggered by stepwise change of the ionic strength of the medium.[5] However, the assembly at the first stage produced a distribution of cluster sizes, including tetramers and hexamers, posing serious limitations to the formation of colloidal crystals in the next stage.[5]

The formation of uniform tetrahedral clusters in a self-limiting way could underpin a bottom-up route to the much sough-after cubic diamond lattice. Despite being an attractive target for programmed colloidal self-assembly, cubic diamond colloidal crystals, which have potential applications as a three-

Received: October 27, 2017
Accepted: February 9, 2018
Published: February 19, 2018

DOI: 10.1021/acsnano.7b07633
ACS Nano 2018, 12, 2355−2364

dimensional complete photonic band gap material,[19,20] have proved remarkably difficult to realize *via* self-assembly. A number of strategies have been explored so far.[21−27] One strategy exploited an interplay between a long-range repulsion and a short-range attraction, both isotropic in nature, at the nanoscale to stabilize a diamond-like open lattice for two oppositely charged nanoparticles.[22] An alternative strategy prescribes the use of anisotropic interactions realized through patchy colloidal particles decorated with four patches in tetrahedral symmetry.[21,24,25] This route faces the challenge of resolving the competition from thermodynamically preferred tetrahedral liquid or gel.[24,25,28] In a related strategy, tetrahedral DNA origami constructs were employed with two types of gold nanoparticles coated with designer single-stranded DNA to form a cubic diamond lattice.[26] However, in this case the spacing between the nanoparticles in the lattice was considerably larger than the core diameter of the nanoparticles, which could restrict its appeal as a photonic crystal.[27] Another distinct route to open structures, such as the cubic diamond lattice, is to first form a denser lattice with two compositionally distinct species each forming a sublattice, one of which is the cubic diamond lattice as in the case for the $MgCu_2$ Laves phase.[23] The removal of the second sublattice selectively produces the cubic diamond lattice as an open structure. This route was followed in a recent work, which employed DNA-mediated interactions to guide preassembled tetrahedral colloidal clusters and spheres to form the $MgCu_2$ Laves phase.[27]

Here we employ a variety of computer simulation techniques to program hierarchical self-assembly, exploiting a hierarchy of interaction strengths. In particular, we demonstrate the hierarchical self-assembly of triblock patchy particles into a cubic diamond lattice *via* tetrahedral clusters, thus underpinning a strategy for its experimental realization. Additionally, for a wider patch width and a longer patch−patch interaction range, we show that these triblock patchy particles self-assemble into a body-centered cubic crystal with a two-level structural hierarchy *via* octahedral clusters, thus lending generality to this design principle.

RESULTS AND DISCUSSION

In the present study, we used a hierarchy of patch−patch interactions, $\epsilon_{AA} > \epsilon_{AB} > \epsilon_{BB}$, where ϵ_{ij} is the depth of the potential due to the patch i−patch j interaction when the patches face each other, together with screened electrostatic repulsion between the middle bands. See Methods and Supporting Figure S1 for further details on the interactions between the designer patchy particles that we considered here as well as the computational methods we employed. Figure 1 shows the most stable structures for certain size-selected clusters on the respective potential energy surfaces for two sets of potential parameters: (1) $\epsilon_{AA} = 5$, $\epsilon_{BB} = 1$, $\alpha = 80°$, $\beta = 40°$, $s = 5$, and $\kappa = 100$; (2) $\epsilon_{AA} = 5$, $\epsilon_{BB} = 1$, $\alpha = 85°$, $\beta = 40°$, $s = 1$, and $\kappa = 100$. For both parameter sets, a remarkable two-level structural hierarchy is on display *via* distinct colloidal molecules at the intermediate level in the form of tetrahedra and octahedra, respectively. The parameter space that supports such striking structural hierarchy was determined by the method of basin-hopping global optimization,[29,30] which we employed to find the global minima on the potential energy surface for size-selected clusters. While the key to the observed structural hierarchy is the hierarchy of patch−patch interaction strengths, the morphology of the colloidal molecules, which essentially

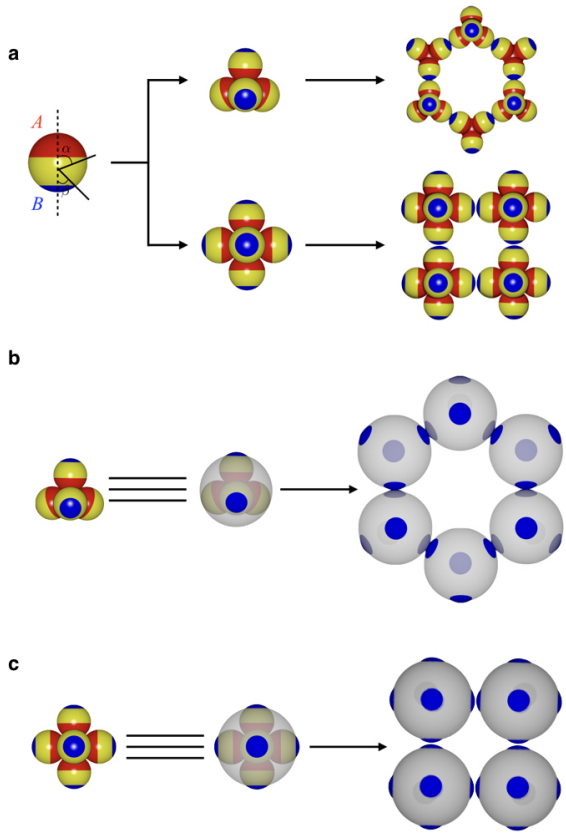

Figure 1. Most stable structures for size-selected clusters of triblock patchy particles under consideration for two sets of model parameters. The set of model parameters includes ϵ_{AA}, ϵ_{BB}, α, β, s, and κ, where ϵ_{ij} is the depth of the potential due to the patch i−patch j interaction when the two patches face each other, α and β are the half-opening angles for patch A and patch B, respectively, κ is the inverse Debye length, and the parameter s controls the range of the patch−patch interactions. (a) For one set, $\epsilon_{AA} = 5$, $\epsilon_{BB} = 1$, $\alpha = 80°$, $\beta = 40°$, $\kappa = 100$, and $s = 5$, a ring-like structure is formed for $N = 24$ with tetrahedral subunits (top). For the other set, $\epsilon_{AA} = 5$, $\epsilon_{BB} = 1$, $\alpha = 85°$, $\beta = 40°$, $\kappa = 100$, and $s = 1$, octahedral subunits appear in a structure of 4-fold symmetry for $N = 48$ (bottom). (b) Ring structure in a reduced representation, showing spheres with tetrahedral patches centered at the geometric centers of the tetrahedral subunits and having the same orientations. (c) Structure with 4-fold symmetry in a reduced representation, showing spheres with octahedral patches centered at the geometric centers of the octahedral subunits and having the same orientations.

serve as the secondary building blocks, is governed by the width of the stronger patch and the range of the patch−patch interactions. A longer range for the patch−patch interactions, indicated by a smaller value of the parameter s (see Supporting Figure S1), and a slightly larger width for the stronger patch favor increased coordination, resulting in the formation of larger clusters at the intermediate level. The closed-loop structure formed with the tetrahedral clusters, as shown in Figure 1, resembles a six-membered ring in terms of the secondary building blocks in the so-called "chair" form. The "boat" form was also found with negligible difference in potential energy (see Supporting Figure S2). The formation of such ring structures suggested the appealing prospect of hierarchical self-assembly of the patchy particles into open

DOI: 10.1021/acsnano.7b07633
ACS Nano 2018, 12, 2355−2364

lattices with local tetrahedral order,[31] especially diamond crystals.[21,25,27,32]

In the context of the promising results obtained in global optimization runs for size-selected clusters, it was imperative that the assembly of these patchy particles be studied in periodic systems, while gradually decreasing the reduced temperature T^*. In the following, we present our results obtained from two series of virtual-move Monte Carlo (VMMC) simulations of $N = 500$ patchy particles in periodic systems at two different volume fractions, one for each set of potential parameters, to unambiguously validate our design principle. In Figure 2, we show the results for the first set of potential parameters at the volume fraction $\phi = 0.2$. Visual inspection revealed the formation of tetrahedral clusters *via* patch A−patch A interactions. We identified these tetrahedral clusters by means of a local order parameter q.[33] As T^* was gradually lowered, concomitant with the drop in the average potential energy per particle, we observed a growth in the number of tetrahedral clusters N_{Td} as shown in Figure 2a. It is remarkable that the tetrahedral clusters were eventually formed in nearly 100% yield; such a self-limited assembly producing clusters of uniform size and shape is a crucial step for hierarchical self-assembly.[15] Figure 2a also shows that the average energy per particle, $V/(N\epsilon_Y)$, rather gradually decreases with the growth in N_{Td} through an intermediate range of values for T^* before showing a small discontinuity at a lower value of T^*. This discontinuous change was an indication for a structural transition taking place.

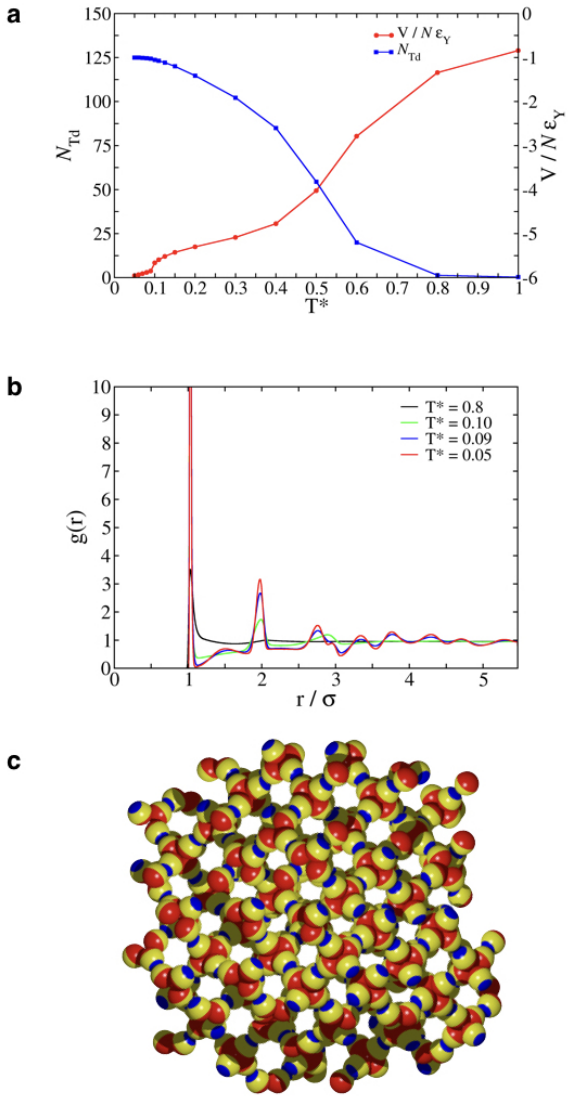

Figure 2. Two-level structural hierarchy *via* tetrahedra emerging from the hierarchical self-assembly of patchy triblock colloidal particles. (a) Average potential energy per particle in the reduced unit, $V/(N\epsilon_Y)$, and the number of tetrahedral clusters formed, N_{Td}, shown on two different scales, as a function of the reduced temperature T^* for an $N = 500$ particle system at the volume fraction $\phi = 0.2$. (b) Pair distribution function $g(r)$ for the patchy particles at four different reduced temperatures. (c) Snapshot of a typical configuration at $T^* = 0.05$, illustrating a two-level structural hierarchy into a colloidal crystal *via* tetrahedra.

We calculated the pair distribution function, which is shown in Figure 2b at certain representative temperatures, in order to characterize this structural transition. At $T^* = 0.09$, long-range correlations develop, indicating the emergence of a long-range order, which becomes more pronounced as T^* is further lowered. A snapshot of a typical configuration at $T^* = 0.05$, shown in Figure 2c, reveals crystalline order, which is also evident in Figure 3a, where we use a reduced representation for clarity. In this reduced representation, we replace the tetrahedral clusters formed at the first level of assembly with spheres having four patches arranged tetrahedrally, their geometric centers coinciding and their orientations kept identical. The second level of assembly was driven by the weaker patch B−patch B interactions. The smaller patch width of patch B resulted in fewer "bonds" formed *via* these interactions; each patch B in fact formed only one bond with another patch B. Since the range of patch−patch interactions was taken to be identical for both patches A and B, the second level of assembly also resulted in a particularly pronounced first peak in the pair distribution function, which continued to become stronger with the enhancement of the crystalline order below $T^* = 0.09$.

In Figure 3b, we show the pair distribution function calculated with the geometric centers of the tetrahedral clusters, present in nearly 100% yield, at certain representative values of T^* along with the pair distribution function for a perfect cubic diamond lattice. Supporting Figure S3 shows a perfect cubic diamond lattice, which can be viewed as a face-centered cubic lattice with half of its tetrahedral sites occupied, in our reduced representation. It is evident that the peaks are centered around those characteristic of a perfect cubic diamond crystal (relative heights not shown) for an appropriately adjusted unit cell length. The probability distribution of the complex conjugate scalar product between the local bond order parameters of two neighboring particles i and j, $\boldsymbol{q}_3(i)\cdot\boldsymbol{q}_3^*(j)$, is shown in Figure 3c. The distribution with a peak around −1 is characteristic of a cubic diamond crystal as opposed to a hexagonal diamond crystal, which, in addition, has a characteristic peak around −0.115.[25]

We now present the results for the second parameter set at the volume fraction $\phi = 0.3$, for which our global optimization runs identified the global minimum with repeating octahedral units for the $N = 48$ cluster as shown in Figure 1. Figure 4a shows that the average energy per particle gradually falls with the drop of T^* as the patchy particles form bonds *via* the stronger and wider patches, resulting in the formation of discrete octahedral clusters. We characterized the octahedral clusters by means of the local order parameter q.[34] The number

DOI: 10.1021/acsnano.7b07633
ACS Nano 2018, 12, 2355−2364

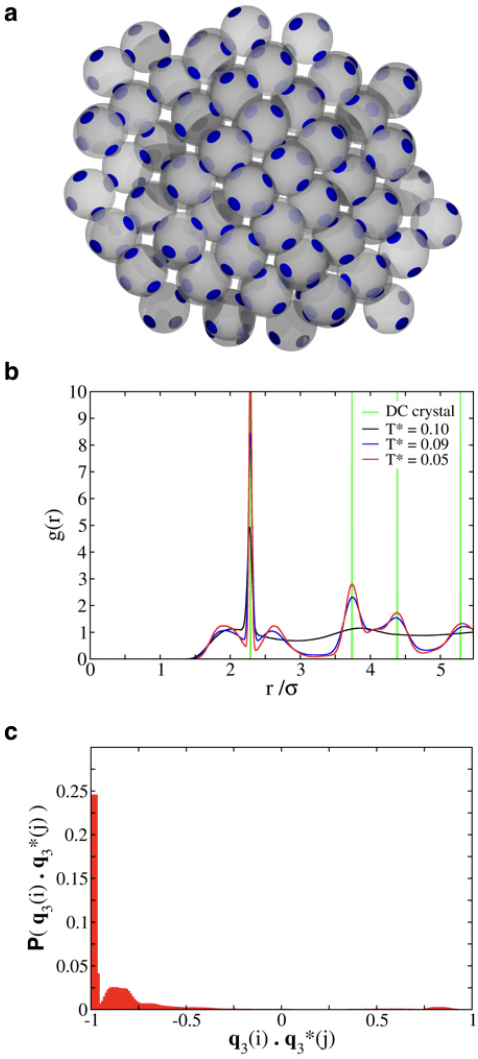

Figure 3. Hierarchical self-assembly of patchy triblock colloidal particles into a cubic diamond crystal *via* tetrahedral clusters. (a) Snapshot of a typical configuration at $T^* = 0.05$ in a reduced representation showing a cubic diamond crystal formed by tetrahedra. (b) Pair distribution function $g(r)$ for the geometric centers of the tetrahedral clusters for configurations at three different temperatures and for a configuration corresponding to a perfect cubic diamond crystal. (c) Probability distribution of the complex conjugate scalar product between the local bond order parameters of two neighboring particles i and j, $q_3(i)\cdot q_3^*(j)$, for the configurations at $T^* = 0.05$. A peak around −1 is a characteristic of a cubic diamond lattice.

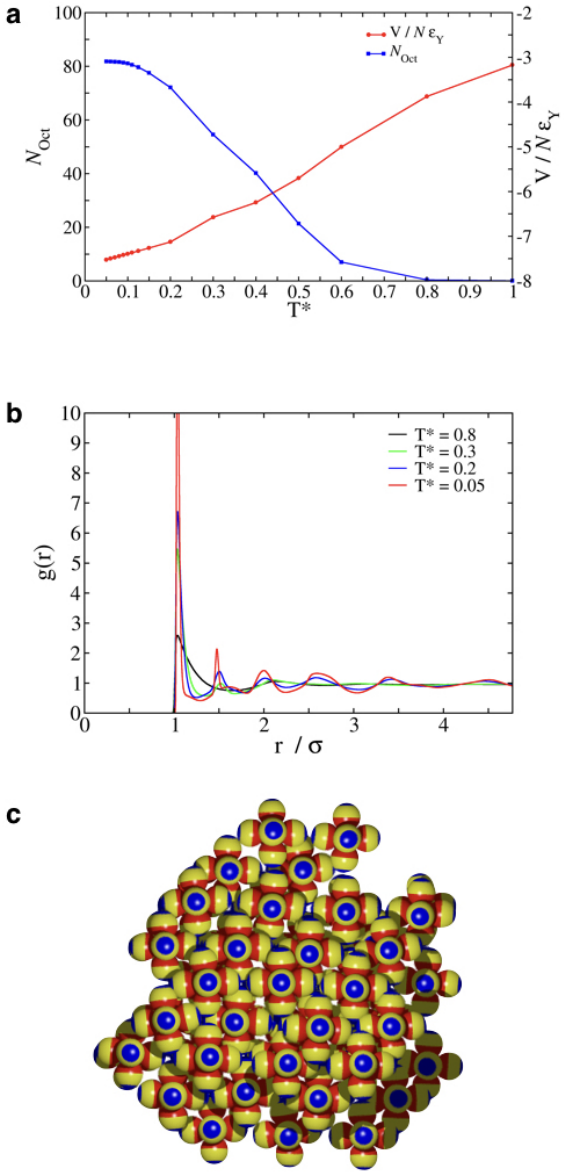

Figure 4. Two-level structural hierarchy *via* octahedra emerging from the hierarchical self-assembly of patchy triblock colloidal particles. (a) Average potential energy per particle in the reduced unit, $V/(N\epsilon_Y)$, and the number of octahedra formed, N_{Oct}, shown on two different scales, as a function of the reduced temperature T^* for an $N = 500$ particle system at the volume fraction $\phi = 0.3$. (b) Pair distribution function $g(r)$ for the patchy particles at four different reduced temperatures. (c) Snapshot of a typical configuration at $T^* = 0.05$, illustrating a two-level structural hierarchy into a colloidal crystal *via* octahedra.

of octahedral clusters in the system gradually grows, and eventually the system effectively consists of octahedral clusters formed again in nearly 100% yield. The pair distribution function for the patchy particles reveals the emergence of long-range correlations at $T^* = 0.2$, implying a second level of assembly of octahedral clusters *via* the interaction of the weaker and narrower patches (Figure 4b). This is confirmed by visual inspection. A typical low-temperature configuration is shown in two different representations (Figure 4c and Figure 5a), which suggest that the octahedral clusters behave as the secondary building blocks for the second level of assembly.

We calculated the pair distribution function for the geometric centers of the octahedral clusters, present in nearly 100% yield, at low values of T^*. In this analysis, we also observed an emergence of long-range correlations at $T^* = 0.2$ (Figure 5b). At this value of T^*, the peaks are centered around those characteristic of a perfect body-centered cubic (bcc) crystal (relative heights not shown) for an appropriately adjusted unit cell length. This observation implies the formation of a bcc crystal by the octahedral clusters at the second level of assembly. This was confirmed by our analysis in terms of the local bond-orientational order parameters $\bar{q}_l(i)$ for $l = 4$ and 6. We considered the distributions of $\bar{q}_4$ and $\bar{q}_6$ calculated for individual centers of octahedral clusters.[35] The distributions, shown in Figure 5c, are consistent with those of a bcc crystal,

DOI: 10.1021/acsnano.7b07633
ACS Nano 2018, 12, 2355−2364

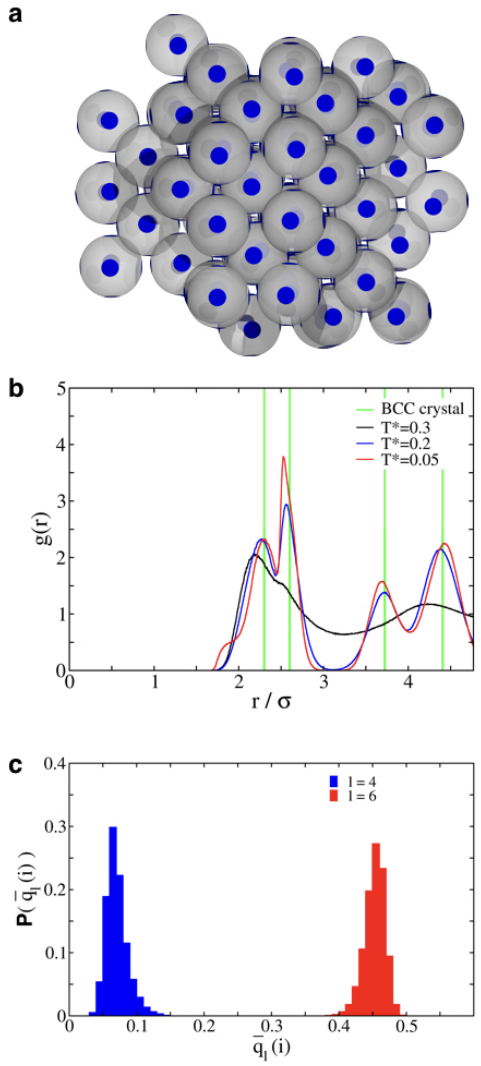

Figure 5. Hierarchical self-assembly of patchy triblock colloidal particles into a body-centered cubic crystal *via* octahedral clusters. (a) Snapshot of a typical configuration at $T^* = 0.05$ in a reduced representation showing a body-centered cubic crystal formed by octahedra. (b) Pair distribution function $g(r)$ for the geometric centers of the octahedral clusters for configurations at three different temperatures and for a configuration corresponding to a perfect body-centered cubic crystal. (c) Probability distribution of the local bond-orientational order parameters $\bar{q}_l(i)$ for $l = 4$ and 6 for octahedral subunits for the configurations at $T^* = 0.05$. The distributions are characteristics of a body-centered cubic lattice.

providing confirmation to our analysis in terms of the pair distribution function for the geometric centers of the octahedral clusters. Given that the range of the patch−patch interactions is relatively longer in this case corresponding to a smaller value of the parameter s, such interactions are more likely to be realizable with nanoscale building blocks. It is of interest to note that nano-octahedra with short-range repulsive interactions were found to self-assemble into a bcc crystal,[36] and so do nearly perfect octahedra obtained *via* truncation of hard tetrahedra at low densities.[37]

We thus exploited a hierarchy of interaction strengths to encode a two-level structural hierarchy and employed gradual temperature control to induce the self-assembly into colloidal crystals with such structural hierarchy. It was then of interest to explore whether a two-step temperature-control protocol would suffice to result in the formation of such crystals. We indeed observed that a two-step temperature-control protocol in VMMC simulations led to the crystal formation, allowing for the two-level assembly to take place, as shown in Figure 6. We chose to reduce T^* in the first step to 0.2, where the tetrahedral clusters were observed in ∼90% yield in the case of gradual cooling (Figure 2a) and then to 0.09 in the second step. The pair distribution function calculated with the geometric centers of the tetrahedral clusters, shown in Figure 6a, highlights the emergence of long-range order upon the second step of rapid cooling, as also confirmed by visual inspection (Figure 6c,d). The probability distribution of the complex conjugate scalar product $\boldsymbol{q}_3(i)\cdot\boldsymbol{q}_3^*(j)$, shown in Figure 6b, confirms a cubic diamond structure. The success of this two-step temperature-control protocol to induce the self-assembly of the cubic diamond crystal with a two-level structural hierarchy led us to exploit such a protocol to assess the robustness of the assembly behavior over the parameter space, which is rather large. Some systematic variation of the parameters around the first set of parameters in particular was undertaken because of special interest in bottom-up realization of a cubic diamond colloidal crystal. Given the span of the parameter space, this scan was not exhaustive. Our results, summarized in Supporting Table S1 in the Supporting Information (see also accompanying discussion), nevertheless show that a reasonable spread of the parameter space supports the two-level self-assembly behavior into cubic diamond crystals *via* tetrahedral clusters.

It is remarkable that a cluster phase with uniform clusters is observed for the systems considered here, unlike the polydisperse clusters observed in the experimental study reported in ref 5. This monodispersity is crucial for the cluster phase to serve as the precursor for crystallization. The patch size of the bigger patch A, expressed in terms of the half-opening angle α, is a crucial design parameter along with the range of the patch−patch interactions, governed by the parameter s, to control the size and shape of the clusters formed. For $\alpha = 80°$ instead of $\alpha = 85°$ with the remaining parameters as in the second set including $s = 1$, we observed a mixture of tetrahedral and octahedral clusters in bulk simulations (see Supporting Figure S4). However, the global optimization runs for a finite-size system of $N = 48$ particles found the most stable structure to be consisting of only octahedral repeat units for this set of parameters with $\alpha = 80°$ and $s = 1$. For larger values of $s \geq 2$, only tetrahedral clusters were observed for finite systems in global optimization runs. The triblock patchy particles that we considered here resemble closely those synthesized by Chen *et al.* with asymmetric patch sizes.[5] We note here that the triblock patchy particles synthesized had an A patch with $\alpha = 60°$ and a B patch with $\beta = 40°$ half-opening angle.[5] Our results thus suggest that the patch size of the wider patch was suboptimal for the first stage of the assembly to produce monodisperse clusters in this experimental work. It is also plausible that the range of the patch−patch interactions also had a role to play.

The experimentally synthesized particles involved screened Coulomb interactions due to the charged middle bands and short-ranged hydrophobic attractions between the patches.[5] We chose a hierarchy of interaction strengths for the distinct patch−patch interactions to trigger staged assembly *via* temperature control. For particles with a diameter of 1 μm, the κ values used here amount to a range of values for the Debye length, which is well within the experimentally accessible

DOI: 10.1021/acsnano.7b07633
ACS Nano 2018, 12, 2355−2364

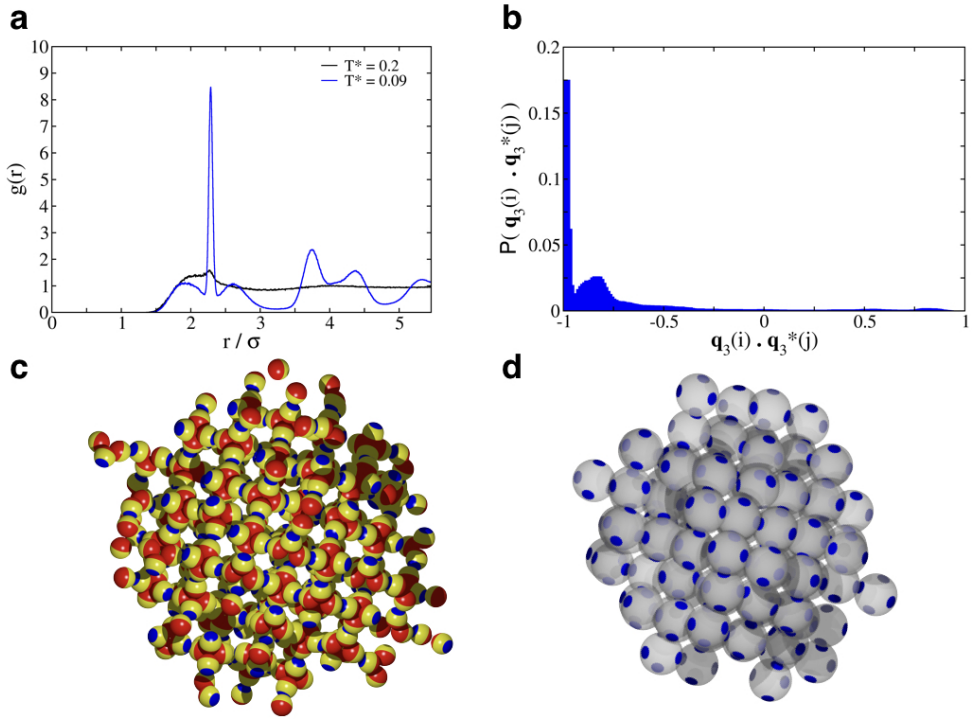

Figure 6. Self-assembly of triblock patchy particles into a cubic diamond crystal upon following a two-step temperature-control protocol. (a) **Pair distribution function $g(r)$ for the geometric centers of the tetrahedral clusters at $T^* = 0.2$ (black) and $T^* = 0.09$ (blue).** (b) **Probability distributions of the complex conjugate scalar product between the local bond order parameters of two neighboring particles i and j, $\tilde{q}_3(i)\cdot\tilde{q}_3^*(j)$, for the configurations at $T^* = 0.09$.** (c, d) **Snapshots of a typical configuration with long-range order at $T^* = 0.09$, showing** (c) **the triblock patchy particles and** (d) **a reduced representation for the tetrahedra formed at the first level of assembly.**

regime. Our bulk simulations also reveal that the ratio $\epsilon_{AA}/\epsilon_{BB}$ is crucial for the second level of assembly. For $\epsilon_{AA} = 5$ and $\epsilon_{BB} = 2.5$, we did not observe any crystalline order at lower values of T^* for either of the two sets of model parameters; instead we observed disordered structures mostly with secondary building blocks. This observation is in line with the findings reported in ref 17. A weaker interaction strength drives the second level of assembly efficiently *via* reversible bond formation, which allows the kinetic traps due to wrong contacts to be negotiated effectively.

Chen *et al.* suggest that the triblock patchy particles considered in their experimental work can nowadays be synthesized with high fidelity and monodispersity, including fairly precise control on the patch sizes.[5] The patch size was uniform within an uncertainty of less than 5° for the triblock patchy particles they synthesized.[5] We therefore considered Gaussian distributions for patch sizes, having mean values of 80° and 40° for patch A and patch B, respectively, and each having a standard deviation of 5/3°, in order to allow for some polydispersity. We followed the two-step temperature-quench protocol with polydispersity in both patches, keeping the remaining parameters of the first set identical. Similarly, we considered polydispersity in both patches corresponding to the second set of parameters, *i.e.*, with Gaussian distributions for patch sizes, having mean values of 85° and 40° for patch A and patch B, respectively, and each having a standard deviation of 5/3°. In both cases, a rapid cooling protocol (three steps in the first case and two steps in the second case) led to the emergence of crystalline order similar to what we observed for the monodisperse case (see Supporting Figure S5). Our results therefore demonstrate that our bottom-up route to colloidal crystals with a two-level structural hierarchy self-assembled from triblock patchy particles shows some tolerance to polydispersity in the patch sizes comparable to the state-of-the-art fabrication.

In addition to VMMC simulations of $N = 500$ patchy triblock colloidal particles, Brownian dynamics (BD) simulations of a system of $N = 864$ particles were also undertaken. It was necessary to carry out BD simulations in order to conclusively determine whether the dynamical pathways involve stagewise assembly. A pertinent question was whether a cluster-move algorithm such as VMMC biased the system here to form clusters in the first instance based on energetics and thus favored staged assembly. Although VMMC can be used to approximate real dynamics for an appropriate choice of parameters, here VMMC was implemented primarily for the enhanced sampling from equilibrium distribution, achieved through cluster moves. Figure 7 shows the results obtained from the BD simulations. Figure 7a shows the number of tetrahedra formed in the BD simulations upon cooling and also compares the evolution of the average potential energy per particle $V/(N\epsilon_Y)$ for BD and VMMC simulations, as a function of T^*. As previously stated, tetrahedral clusters were identified using the local order parameter q. Here, tetrahedral clusters were again formed in near 100% yield, crucial for the next stage of self-assembly. Furthermore, the correspondence of the average potential energy per particle, $V/(N\epsilon_Y)$, in both simulation methods, except at very low T^* values, is noteworthy, implying an effective sampling at thermal equilibrium by both methods over most of the temperature range. A gradual decrease in the average potential energy per particle was observed for intermediate values of T^* along with a small discontinuity at lower values of T^* in the BD simulations. As with the VMMC simulations, the discontinuous change was

DOI: 10.1021/acsnano.7b07633
ACS Nano 2018, 12, 2355−2364

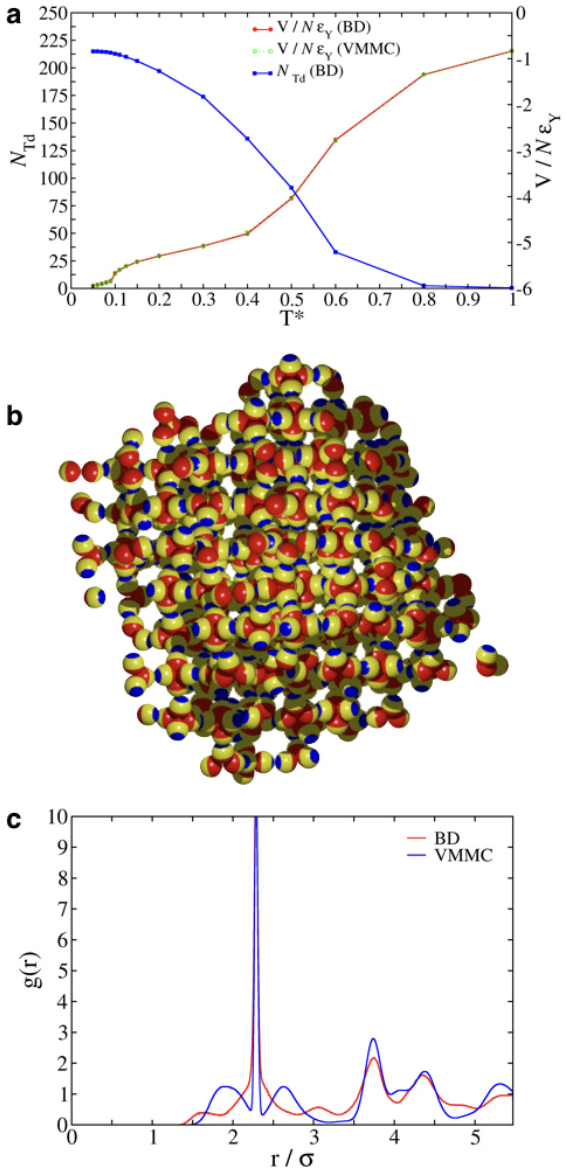

Figure 7. Two-level hierarchical self-assembly of triblock patchy particles observed in Brownian dynamics simulations. (a) Average potential energy per particle in the reduced unit, $V/(N\epsilon_Y)$, and the number of tetrahedral clusters, N_{Td}, on two different scales, as a function of the reduced temperature T^*, for an $N = 864$ particle system at a volume fraction of $\phi = 0.2$. (b) Snapshot of a typical configuration at $T^* = 0.05$, displaying two-level structural hierarchy. (c) Pair distribution function $g(r)$ for the geometric centers of tetrahedral clusters at $T^* = 0.05$.

an indicator for a structural change taking place. Figure 7b shows a snapshot of a typical configuration at $T^* = 0.05$ for the BD simulations. Although not as ordered as observed in VMMC simulations (Figure 2c), a degree of crystalline order within the $N = 864$ system can be discerned. This was confirmed upon calculation of the pair distribution function for the geometric centers of the tetrahedral clusters, shown in Figure 7c. In Figure 7c the pair distribution function obtained from the BD simulations is also compared to that obtained from the VMMC simulations. The emergence of long-range order was also observed in BD simulations. In addition, the pair distribution functions compare reasonably well and exhibit peaks at positions characteristic of a cubic diamond lattice. Our BD simulations thus unequivocally demonstrate hierarchical self-assembly of triblock patchy particles into a cubic diamond lattice.

CONCLUSION

In summary, we have explored a design rule that prescribes the use of a hierarchy of interaction strengths to program hierarchical self-assembly of colloidal building blocks and demonstrated its generality in computer simulations, mostly employing a sophisticated cluster-move Monte Carlo algorithm. Such a generic design rule for hierarchical self-assembly can be exploited to fabricate colloidal superstructures of great complexity. In particular, we exploited the design principle, realized with triblock patchy particles that closely resemble those synthesized recently,[5] to show hierarchical self-assembly into a cubic diamond colloidal crystal and a body-centered cubic colloidal crystal *via* tetrahedral and octahedral clusters, respectively. The use of colloidal building blocks with only two patches to form a cubic diamond colloidal crystal *via* a hierarchical self-assembly scheme makes it a promising route for the experimental realization of photonic crystals with a band gap in the visible region in the foreseeable future. This route relaxes the stringent requirement on the fidelity of particle synthesis associated with the fabrication of precisely tetrahedral patches.[38] In the presence of a hierarchy of interaction strengths, the two-level self-assembly was triggered by gradually lowering the temperature; our results further show that a two-step temperature-control protocol could also be judiciously employed. We also show that the design principle being exploited here shows tolerance to polydispersity in the patch sizes comparable to the state-of-the-art fabrication. Finally, we present results from Brownian dynamics simulations, which unequivocally demonstrate that the triblock patchy particles undergo stagewise assembly into a cubic diamond lattice *via* tetrahedral clusters. Such dynamical pathways offer the opportunity for investigating nonclassical pathways to colloidal crystals with structural hierarchy.[39]

METHODS

Model. We employed the traditional one-component description for the colloidal suspensions considered here with a pairwise effective potential.[40] In this description, triblock patchy colloidal particles are modeled as rigid bodies consisting of a spherical core decorated with two distinct patches, A and B, located on opposing poles across a charged middle band. The effective potential has an isotropic component in the form of the Yukawa potential describing screened electrostatic repulsion and an anisotropic component, which describes the directional interactions between patches. In our model, both patches A and B are able to interact with themselves and one another. Patches A and B differ in terms of their surface coverage, characterized by the angles α and β, which describe their half-patch widths, respectively, and the strength of their patch−patch interactions. ϵ_{ij} is the depth of the potential due to the patch i−patch j interaction when the two patches face each other. The effective potential for a pair of patchy particles V is given by

$$V(\boldsymbol{r}_{ij}, \boldsymbol{\Omega}_i, \boldsymbol{\Omega}_j) = U_Y(r_{ij}) + \sum_{p\in i}\sum_{p'\in j} U_{pp'}(\boldsymbol{r}_{ij}, \boldsymbol{\Omega}_i, \boldsymbol{\Omega}_j)\, w_{pp'}(r_{ij}) \quad (1)$$

where $\boldsymbol{r}_{ij} = \boldsymbol{r}_j - \boldsymbol{r}_i$ is the separation vector between triblock patchy particles i and j, $\boldsymbol{r}_i$ is the position vector for the geometric center of the patchy particle i, and r_{ij} is the magnitude of the vector $\boldsymbol{r}_{ij}$. $\boldsymbol{\Omega}_i$ and $\boldsymbol{\Omega}_j$ describe the orientations of particles i and j, respectively. The isotropic component U_Y is the repulsive Yukawa potential:

DOI: 10.1021/acsnano.7b07633
ACS Nano 2018, 12, 2355−2364

$$U_Y(r_{ij}) = \epsilon_Y \frac{\exp[-\kappa(r_{ij} - \sigma)]}{r_{ij}/\sigma} \quad (2)$$

where κ is the inverse Debye screening length and ϵ_Y is the Yukawa contact potential.

The angular dependence of the patch−patch interaction is described by $U_{pp'}$:[41]

$$U_{pp'}(\mathbf{r}_{ij}, \mathbf{\Omega}_i, \mathbf{\Omega}_j) = \epsilon_{pp'} \frac{1}{4}[1 + \Phi(\mathbf{r}_{ij}, \mathbf{\Omega}_i, \mathbf{p}_i)][1 + \Phi(\mathbf{r}_{ji}, \mathbf{\Omega}_j, \mathbf{p}_j)] \quad (3)$$

$$\Phi(\mathbf{r}_{ij}, \mathbf{\Omega}_i, \mathbf{p}_i) = \begin{cases} -1, & \cos\theta_{ijp_i} < \cos\delta, \\ -\cos\left(\dfrac{\pi[\cos\theta_{ijp_i} - \cos\delta]}{1 - \cos\delta}\right), & \cos\theta_{ijp_i} \geq \cos\delta \end{cases} \quad (4)$$

The depth of the patch−patch interaction is given by $\epsilon_{pp'}$. Here $\mathbf{p}_i$ is a normalized vector from the center of the spherical particle i in the direction of the patch p on it, which depends on $\mathbf{\Omega}_i$, and $\cos\theta_{ijp_i}$ is the scalar product of the normalized vector $\hat{\mathbf{r}}_{ij}$ with $\mathbf{p}_i$. The width of the patch is controlled by the parameter $\cos\delta$, where δ is the half-opening angle.

The distance dependence of the patch−patch interaction is governed by the function $w_{pp'}$:

$$w_{pp'}(r_{ij}) = \begin{cases} -1, & \text{if } (r_{ij} - \lambda) < 0, \\ -\dfrac{1}{2}[1 + \cos(\pi(r_{ij} - \lambda)s)], & \text{if } 0 \leq (r_{ij} - \lambda) \leq s^{-1}, \\ 0, & \text{if } (r_{ij} - \lambda) > s^{-1} \end{cases} \quad (5)$$

where λ is the largest separation at which the patch p−patch p' attraction is at its strongest and the parameter s controls the range over which this attraction decreases to zero. In the present study, λ was set to 1.01σ. We used reduced units: the length in the units of σ, the energy in the units of ϵ_Y, and the temperature in the units of ϵ_Y/k_B. In the absence of a hard core σ provides an estimate for the size of the charge-stabilized patchy particles. We set $\epsilon_{AB} = \sqrt{\epsilon_{AA}\epsilon_{BB}}$.

Structure Prediction for Clusters. We employed the basin-hopping global optimization method,[29,30] as implemented in GlOSP, a program for Global Optimization for Structure Prediction developed in-house, to identify the global minima on the potential energy surface for size-selected clusters. The global minima are the candidates for thermodynamically favored structures observed under experimental conditions especially at low temperatures. The basin-hopping algorithm can be viewed as Monte Carlo plus minimization.[29] An angle-axis representation was used for rigid-body rotational coordinates.[42] The limited-memory Broyden−Fletcher−Goldfarb−Shanno algorithm was used for local minimization with analytic first derivatives of the potential energy.[43] For each set of potential parameters, we carried out five independent runs, starting from five random initial configurations. The runs consisted of 5×10^6 basin-hopping steps for the first set of parameters and 5×10^5 steps for the second one.

Monte Carlo Simulations. A series of virtual-move Monte Carlo simulations were performed in the canonical ensemble with $N = 500$ triblock patchy particles. The simulations were carried out in a cubic box under periodic boundary conditions using the minimum image convention. We employed the symmetrized version of the VMMC algorithm,[44,45] as implemented in PaSSion, a Package for Soft Matter Simulation developed in-house, following a recent prescription.[46] The orientational degrees of freedom were represented by quaternions. Each VMMC cycle consisted of N translation or collective rotational cluster moves, chosen at random with equal probability. The maximum step size for both the translational and collective rotational cluster moves was fixed, taken as $\delta = 0.1$ in the reduced unit and $\theta_{max} = 0.1$, respectively. The potential energy was calculated using a spherical cutoff of radii 1.3 and 2.1 for the sets of potential parameters with $s = 5$ and 1, respectively. A neighbor list was used for efficiency. The systems were equilibrated from an initial face-centered lattice at $T^* = 1$, and T^* was gradually reduced. At each T^* value studied, at least 1×10^6 VMMC cycles were used for equilibration, which was followed by a production stage consisting of 5×10^5 cycles for high values of T^* and 1.5×10^6 cycles for lower values of T^*.

Brownian Dynamics Simulations. A series of Brownian dynamics simulations were also carried out with $N = 864$ triblock patchy particles. A cubic box was used with periodic boundary conditions using the minimum image convention. The Brownian dynamics simulations were performed in the overdamped limit following an algorithm for spherical particles with orientational degrees of freedom represented by a unit vector,[47] ignoring hydrodynamic correlations and translation−rotation coupling. We used appropriate Stokes laws with sticky boundary conditions for the translational and rotational diffusion coefficients at infinite dilution. For BD simulations, the time was expressed in units of σ^2/D_0^t, where D_0^t is the translational diffusion coefficient at infinite dilution. The system was equilibrated from an initial face-centered lattice at $T^* = 1$, and T^* was gradually reduced. At each value of T^* studied, a minimum of 1×10^7 steps, going up to 4.35×10^9 at certain low temperatures, were used for equilibration, followed by a production stage of at least 1×10^7 steps. Below a reduced temperature of $T^* = 0.10$ a time step of $\Delta t = 5 \times 10^{-6}$ in the reduced unit was used; for all other values of T^*, a time step of $\Delta t = 10^{-6}$ in the reduced unit was used.

Bond-Orientational Order Parameters. We calculated various local bond-orientational order parameters based on spherical harmonics as diagnostics for crystal structures.[48,49] In this analysis, a complex vector $\boldsymbol{q}_l(i)$, having $2l + 1$ components, is assigned to each particle i. The mth unnormalized component of $\boldsymbol{q}_l(i)$ is defined as

$$q_{lm}(i) = \frac{1}{N_b(i)} \sum_{j=1}^{N_b(i)} Y_{lm}(\hat{\boldsymbol{r}}_{ij}) \quad (6)$$

where $N_b(i)$ is the number of neighbors of particle i located within a distance corresponding to the location of the first peak of the radial distribution function and $Y_{lm}(\hat{\boldsymbol{r}}_{ij}) \equiv Y_{lm}(\theta_{ij}, \phi_{ij})$ are the spherical harmonics corresponding to the polar and azimuthal angles, θ_{ij} and ϕ_{ij}, respectively, of the bond $\boldsymbol{r}_{ij}$ between i and its neighbor j.

We calculated the following averaged local bond-orientational order parameters:[35]

$$\bar{q}_l(i) = \sqrt{\frac{4\pi}{2l + 1} \sum_{m=-l}^{+l} |\bar{q}_{lm}(i)|^2} \quad (7)$$

where

$$\bar{q}_{lm}(i) = \frac{1}{\tilde{N}_b(i)} \sum_{k=0}^{\tilde{N}_b(i)} q_{lm}(k) \quad (8)$$

Here, by summing over $k = 0$ to $\tilde{N}_b(i)$ when calculating $\bar{q}_{lm}(i)$, we take into account all of the neighbors of particle i as well as the particle i itself. This averaging process, which considers both the first and the second shell around a particle, was shown to considerably improve the accuracy in distinguishing among crystal structures.[35]

In order to specifically distinguish between the cubic diamond (DC) crystal and hexagonal diamond (DH) crystal, we calculated the complex conjugate scalar product $\tilde{\boldsymbol{q}}_3(i)\cdot\tilde{\boldsymbol{q}}_3^*(j)$.[21,25] For every particle i its four nearest neighbors were considered to define the normalized seven-component complex vector $\tilde{\boldsymbol{q}}_3(i)$ with components

$$\tilde{q}_{3m}(i) = \frac{q_{3m}(i)}{\left[\sum_{m=-3}^{3} |q_{3m}(i)|^2\right]^{1/2}} \quad (9)$$

When the probability distribution of the complex conjugate scalar product $\tilde{\boldsymbol{q}}_3(i)\cdot\tilde{\boldsymbol{q}}_3^*(j)$ is plotted for these two crystals, in their perfect forms both show a peak at −1, but the presence of a peak around

DOI: 10.1021/acsnano.7b07633
ACS Nano 2018, 12, 2355−2364

−0.115 is a signature of the hexagonal diamond crystal.[25] In the perfect DC crystal all four neighbors j of each particle i are arranged such that $\tilde{\mathbf{q}}_3(i)\cdot\tilde{\mathbf{q}}_3^*(j) = -1$, where as for the perfect DH crystal each particle i has three neighbors for which $\tilde{\mathbf{q}}_3(i)\cdot\tilde{\mathbf{q}}_3^*(j) = -1$ and one such that $\tilde{\mathbf{q}}_3(i)\cdot\tilde{\mathbf{q}}_3^*(j) = -0.115$.[25]

Orientational Order Parameters. We first identified clusters of four or six particles in order to determine the number of tetrahedra or octahedra formed in the respective system. The cluster identification was carried out using a threshold value for the distance between centers of patch A on two neighboring particles, below which the particles were taken to belong to the same cluster. While examining a cluster of four or six particles in order to assess whether the particles have a tetrahedral or an octahedral arrangement, we employed the following orientational order parameter q:[33,50]

$$q = 1 - \frac{3}{8}\sum_{j=1}^{N_b-1}\sum_{k=j+1}^{N_b}\left(\cos\psi_{jk} + \frac{1}{3}\right)^2 \tag{10}$$

where N_b is the number of particles in the cluster under consideration and ψ_{jk} is the angle subtended at the center of the cluster by the two vectors joining the center to particles j and k. In the case of a perfect tetrahedron $q = 1$ with $N_b = 4$; for a perfect octahedron $q = 0$ with $N_b = 6$.[34] We used threshold values to identify a cluster as a tetrahedron or an octahedron.

ASSOCIATED CONTENT

Supporting Information

The Supporting Information is available free of charge on the ACS Publications website at DOI: 10.1021/acsnano.7b07633.

Additional information (PDF)

AUTHOR INFORMATION

Corresponding Author

*E-mail: d.chakrabarti@bham.ac.uk.

ORCID

Dwaipayan Chakrabarti: 0000-0002-2939-2808

Notes

The authors declare no competing financial interest.

ACKNOWLEDGMENTS

We thank Qian Chen and Vinothan N. Manoharan for stimulating discussions, facilitated by support received from the Institute of Advanced Studies of the University of Birmingham. D.M. and J.S. gratefully acknowledge support from the Engineering and Physical Sciences Research Council of the UK and the University of Birmingham. D.C. acknowledges support from the North America Travel Fund of the University of Birmingham.

REFERENCES

(1) Glotzer, S. C.; Solomon, M. J. Anisotropy of Building Blocks and their Assembly into Complex Structures. *Nat. Mater.* **2007**, *6*, 557.

(2) Cademartiri, L.; Bishop, K. J. M. Programmable Self-Assembly. *Nat. Mater.* **2015**, *14*, 2−9.

(3) Rogers, W. B.; Shih, W. M.; Manoharan, V. N. Using DNA to Program the Self-Assembly of Colloidal Nanoparticles and Microparticles. *Nat. Rev. Mater.* **2016**, *1*, 364−368.

(4) Miszta, K.; de Graaf, J.; Bertoni, G.; Dorfs, D.; Brescia, R.; Marras, S.; Ceseracciu, L.; Cingolani, R.; van Roij, R.; Dijkstra, M.; Manna, L. Hierarchical Self-Assembly of Suspended Branched Colloidal Nanocrystals into Superlattice Structures. *Nat. Mater.* **2011**, *10*, 872−876.

(5) Chen, Q.; Bae, S. C.; Granick, S. Staged Self-Assembly of Colloidal Metastructures. *J. Am. Chem. Soc.* **2012**, *134*, 11080−11083.

(6) Haxton, T. K.; Whitelam, S. Do Hierarchical Structures Assemble Best via Hierarchical Pathways? *Soft Matter* **2013**, *9*, 6851−6861.

(7) Grünwald, M.; Geissler, P. L. Patterns without Patches: Hierarchical Self-Assembly of Complex Structures from Simple Building Blocks. *ACS Nano* **2014**, *8*, 5891−5897.

(8) Morphew, D.; Chakrabarti, D. Hierarchical Self-Assembly of Colloidal Magnetic Particles into Reconfigurable Spherical Structures. *Nanoscale* **2015**, *7*, 8343−8350.

(9) McGinley, J. T.; Wang, Y.; Jenkins, I. C.; Sinno, T.; Crocker, J. C. Crystal-Templated Colloidal Clusters Exhibit Directional DNA Interactions. *ACS Nano* **2015**, *9*, 10817−10825.

(10) Zanjani, M. B.; Jenkins, I. C.; Crocker, J. C.; Sinno, T. Colloidal Cluster Assembly into Ordered Superstructures via Engineered Directional Bonding. *ACS Nano* **2016**, *10*, 11280−11289.

(11) Morphew, D.; Chakrabarti, D. Clusters of Anisotropic Colloidal Particles: from Colloidal Molecules to Supracolloidal Structures. *Curr. Opin. Colloid Interface Sci.* **2017**, *30*, 70−80.

(12) van Blaaderen, A. Colloidal Molecules and Beyond. *Science* **2003**, *301*, 470−471.

(13) Manoharan, V. N.; Elsesser, M. T.; Pine, D. J. Dense Packing and Symmetry in Small Clusters of Microspheres. *Science* **2003**, *301*, 483−487.

(14) Wang, Y.; Wang, Y.; Breed, D. R.; Manoharan, V. N.; Feng, L.; Hollingsworth, A. D.; Weck, M.; Pine, D. J. Colloids with Valence and Specific Directional Bonding. *Nature* **2012**, *491*, 51−56.

(15) Nguyen, T. D.; Schultz, B. A.; Kotov, N. A.; Glotzer, S. C. Generic, Phenomenological, on-the-fly Renormalized Repulsion Model for Self-Limited Organization of Terminal Supraparticle Assemblies. *Proc. Natl. Acad. Sci. U. S. A.* **2015**, *112*, E3161−E3168.

(16) O'Brien, M. N.; Jones, M. R.; Mirkin, C. A. The Nature and Implications of Uniformity in the Hierarchical Organization of Nanomaterials. *Proc. Natl. Acad. Sci. U. S. A.* **2016**, *113*, 11717−11725.

(17) Morphew, D.; Chakrabarti, D. Programming Hierarchical Self-Assembly of Colloids: Matching Stability and Accessibility. Submitted for publication.

(18) Choi, I. S.; Bowden, N.; Whitesides, G. M. Macroscopic, Hierarchical, Two-Dimensional Self-Assembly. *Angew. Chem., Int. Ed.* **1999**, *38*, 3078−3081.

(19) Ho, K. M.; Chan, C. T.; Soukoulis, C. M. Existence of a Photonic Gap in Periodic Dielectric Structures. *Phys. Rev. Lett.* **1990**, *65*, 3152−3155.

(20) Maldovan, M.; Thomas, E. L. Diamond-structured Photonic Crystals. *Nat. Mater.* **2004**, *3*, 593−600.

(21) Zhang, Z.; Keys, A. S.; Chen, T.; Glotzer, S. C. Self-Assembly of Patchy Particles into Diamond Structures through Molecular Mimicry. *Langmuir* **2005**, *21*, 11547−11551.

(22) Kalsin, A. M.; Fialkowski, M.; Paszewski, M.; Smoukov, S. K.; Bishop, K. J. M.; Grzybowski, B. A. Electrostatic Self-Assembly of Binary Nanoparticle Crystals with a Diamond-like Lattice. *Science* **2006**, *312*, 420−424.

(23) Hynninen, A.-P.; Thijssen, J. H. J.; Vermolen, E. C. M.; Dijkstra, M.; van Blaaderen, A. Self-Assembly Route for Photonic Crystals with a Bandgap in the Visible Region. *Nat. Mater.* **2007**, *6*, 202−205.

(24) Noya, E. G.; Vega, C.; Doye, J. P. K.; Louis, A. A. The Stability of a Crystal with Diamond Structure for Patchy Particles with Tetrahedral Symmetry. *J. Chem. Phys.* **2010**, *132*, 234511.

(25) Romano, F.; Sanz, E.; Sciortino, F. Crystallization of Tetrahedral Patchy Particles *in silico*. *J. Chem. Phys.* **2011**, *134*, 174502.

(26) Liu, W.; Tagawa, M.; Xin, H. L.; Wang, T.; Emamy, H.; Li, H.; Yager, K. G.; Starr, F. W.; Tkachenko, A. V.; Gang, O. Diamond Family of Nanoparticle Superlattices. *Science* **2016**, *351*, 582−586.

(27) Ducrot, E.; He, M.; Yi, G.-R.; Pine, D. J. Colloidal Alloys with Preassembled Clusters and Spheres. *Nat. Mater.* **2017**, *16*, 652−657.

(28) Smallenburg, F.; Sciortino, F. Liquids more Stable than Crystals in Particles with Limited Valence and Flexible Bonds. *Nat. Phys.* **2013**, *9*, 554−558.

(29) Li, Z.; Scheraga, H. A. Monte Carlo-Minimization Approach to the Multiple-Minima Problem in Protein Folding. *Proc. Natl. Acad. Sci. U. S. A.* **1987**, *84*, 6611−6615.

DOI: 10.1021/acsnano.7b07633
ACS Nano 2018, 12, 2355−2364

(30) Wales, D. J.; Doye, J. P. K. Global Optimization by Basin-Hopping and the Lowest Energy Structures of Lennard-Jones Clusters Containing up to 110 Atoms. *J. Phys. Chem. A* **1997**, *111*, 5111−5116.
(31) Mao, X.; Chen, Q.; Granick, S. Entropy Favours Open Colloidal Lattices. *Nat. Mater.* **2013**, *12*, 217−222.
(32) Wang, Y.; Jenkins, I. C.; McGinley, J. T.; Sinno, T.; Crocker, J. C. Colloidal Crystals with Diamond Symmetry at Optical Length-scales. *Nat. Commun.* **2017**, *8*, 14173.
(33) Errington, J. R.; Debenedetti, P. G. Relationship Between Structural Order and the Anomalies of Liquid Water. *Nature* **2001**, *409*, 318−321.
(34) Caravati, S.; Bernasconi, M.; Kühne, T. D.; Krack, M.; Parrinello, M. Coexistence of Tetrahedral- and Octahedral-like Sites in Amorphous Phase Change Materials. *Appl. Phys. Lett.* **2007**, *91*, 171906.
(35) Lechner, W.; Dellago, C. Accurate Determination of Crystal Structures Based on Averaged Local Bond Order Parameters. *J. Chem. Phys.* **2008**, *129*, 114707.
(36) Zhang, J.; Luo, Z.; Quan, Z.; Wang, Y.; Kumbhar, A.; Smilgies, D.-M.; Fang, J. Low Packing Density Self-Assembled Superstructure of Octahedral Pt_3Ni Nanocrystals. *Nano Lett.* **2011**, *11*, 2912−2918.
(37) Damasceno, P. F.; Engel, M.; Glotzer, S. C. Crystalline Assemblies and Densest Packings of a Family of Truncated Tetrahedra and the Role of Directional Entropic Forces. *ACS Nano* **2012**, *6*, 609−614.
(38) Gong, Z.; Hueckel, T.; Yi, G.-R.; Sacanna, S. Patchy Particles Made by Colloidal Fusion. *Nature* **2017**, *550*, 234−238.
(39) De Yoreo, J. J.; Gilbert, P. U. P. A.; Sommerdijk, N. A. J. M.; Penn, R. L.; Whitelam, S.; Joester, D.; Zhang, H.; Reimer, J. D.; Navrotsky, A.; Banfield, J. F.; Wallace, A. F.; Michel, F. M.; Meldrum, F. C.; Cölfen, H.; Dove, P. M. Crystallization by Particle Attachment in Synthetic, Biogenic, and Geologic Environments. *Science* **2015**, *349*, aaa6760.
(40) Bianchi, E.; Blaak, R.; Likos, C. N. Patchy Colloids: State of the Art and Perspectives. *Phys. Chem. Chem. Phys.* **2011**, *13*, 6397−6410.
(41) Morgan, J. W. R.; Chakrabarti, D.; Dorsaz, N.; Wales, D. J. Designing a Bernal Spiral from Patchy Colloids. *ACS Nano* **2013**, *7*, 1246−1256.
(42) Chakrabarti, D.; Wales, D. J. Simulations of Rigid Bodies in an Angle-Axis Framework. *Phys. Chem. Chem. Phys.* **2009**, *11*, 1970−1976.
(43) Liu, D.; Nocedal, J. On the Limited Memory BFGS Method for Large Scale Optimization. *Mathematical Programming* **1989**, *45*, 503−528.
(44) Whitelam, S.; Geissler, P. G. Avoiding Unphysical Kinetic Traps in Monte Carlo Simulations of Strongly Attractive Particles. *J. Chem. Phys.* **2007**, *127*, 154101.
(45) Whitelam, S.; Feng, E. H.; Hagan, M. F.; Geissler, P. G. The Role of Collective Motion in Examples of Coarsening and Self-Assembly. *Soft Matter* **2009**, *5*, 1251−1262.
(46) Růžička, Š.; Allen, M. P. Collective Translational and Rotational Monte Carlo Moves for Attractive Particles. *Phys. Rev. E* **2014**, *89*, 033307.
(47) Mériguet, G.; Jardat, M.; Turq, P. Structural Properties of Charge-Stabilized Ferrofluids under a Magnetic Field: A Brownian Dynamics Study. *J. Chem. Phys.* **2004**, *121*, 6078−6085.
(48) Steinhardt, P. J.; Nelson, D. R.; Ronchetti, M. Bond-Orientational Order in Liquids and Glasses. *Phys. Rev. B: Condens. Matter Mater. Phys.* **1983**, *28*, 784−805.
(49) ten Wolde, P. R.; Ruiz-Montero, M. J.; Frenkel, D. Numerical Calculation of the Rate of Crystal Nucleation in a Lennard-Jones System at Moderate Undercooling. *J. Chem. Phys.* **1996**, *104*, 9932−9947.
(50) Chau, P.-L.; Hardwick, A. J. A New Order Parameter for Tetrahedral Configurations. *Mol. Phys.* **1998**, *93*, 511−518.

DOI: 10.1021/acsnano.7b07633
ACS Nano 2018, 12, 2355−2364